Int. J. Heat Mass Transfer. Vol. 33, No. 6, pp. 1263–1280, 1990
Printed in Great Britain

0017-9310/90 $3.00+0.00

A synthesis of infiltration effects on an insulation matrix

H. C. TIEN and K. VAFAI
Department of Mechanical Engineering, Ohio State University, Columbus, OH 43210, U.S.A.

(*Received* 10 *May* 1989 *and in final form* 5 *September* 1989)

Abstract—This work presents the effects of air infiltration on heat and mass transfer in a porous matrix. The vertical boundaries of the porous system are partially permeable in order to simulate the holes or the cracks in the porous insulation materials. An efficient numerical scheme accounting for phase change is employed to solve the appropriate governing equations along with the boundary conditions, which describe the complicated transport process. The interactions of the field variables and the influence of the Biot numbers and the opening size are investigated. The effects of the locations of the openings on the Nusselt number are researched through investigating four representative cases. In all cases, it is found that the liquid accumulates heavily in the region which is exposed to the hot and humid environment. It is also found that infiltration plays a very important role in determining the overall heat transfer rates as well as the generated liquid condensate.

1. INTRODUCTION

SEVERAL studies in the heat transfer literature fall within the general area of heat and mass transfer in porous media with or without phase change. Some of the studies, such as Phillip and Devries [1], Devries [2], Luikov [3], and Whitaker [4] presented general formulations of these types of problems, while some of the other works are related to more specific applications. In the latter category, the subject of drying in a porous material has received considerable attention. For example, Ceaglske and Hougen [5] investigated the drying of granular porous media and found that the drying rate is determined not by diffusion but by capillary forces; Berger and Pei [6] proposed a mathematical model of drying, taking both vapor diffusion and capillary liquid flow as well as heat transfer through solids into account; Whitaker and Chou [7] constructed a simplified theory for drying granular porous media, and Kaviany and Mittal [8] investigated the drying of a non-hygroscopic porous slab initially saturated with liquid up to the critical time. Reddy *et al.* [9] analyzed the heat and mass transfer in soils with heat sources. Udell and Fitch [10, 11] investigated the heat transfer in porous media with phase change and capillarity—the heat pipe effect. Also, Eckert and Faghri [12] and Dinulescu and Eckert [13] studied the one-dimensional moisture migration caused by temperature gradients in a porous medium. Both studies by Eckert and Faghri [12], and Dinulescu and Eckert [13] are related to the problems such as the moisture redistribution in soil under the influence of solar heat. The interest in the subject of simultaneous heat and mass transfer in porous media has continuously increased in recent years since it has become more apparent that many applications in thermal engineering require a good working knowledge of this subject.

An interesting topic, from the fundamental and applied point of view is condensation in porous insulations. The heat and moisture transport in a porous insulation is a multi-dimensional problem with multi-component (air–vapour mixture) flow. In general, a wet porous insulation consists of three phases. These are the solid matrix, the liquid water, and a binary gas phase composed of air and vapor. The transport mechanisms involved in the process are quite complicated. In the gas phase, there is vapor diffusion due to the vapor concentration gradients, bulk convection due to the density variation induced by temperature gradients, and air infiltration due to the small difference in gas pressure across the insulation. There is heat conduction in all three phases and heat convection in the gas phase. There will also be convection in the liquid phase if it is mobile. In addition, there is heat transfer caused by phase change at the gas–liquid interface. The above-mentioned phenomena present complex interactions between heat and mass transport mechanisms.

Most of the experimental studies on this subject such as Tye and Spinney [14], Stewart [15] and Langlais *et al.* [16] were conducted for some specific applications. Analytical and numerical studies were also carried out such as a one-dimensional quasi-steady semi-analytical approach by Ogniewicz and Tien [17], a one-dimensional transient numerical study by Vafai and Sarkar [18] and a two-dimensional unsteady numerical work with simplifying assumptions by Vafai and Whitaker [19]. The major investigation in studying the infiltration effects without accounting the condensation or the multi-component effects has been done by Burns *et al.* [20] and by Burns

NOMENCLATURE

A	aspect ratio, $\bar{H}/\bar{L}$
B	Biot number referring to heat transfer, $\bar{h}\bar{L}/\bar{k}_{\text{eff},0}$
B^*	Biot number referring to mass transfer, $\bar{h}^*\bar{L}/\bar{\alpha}_{\text{eff},0}$
B_v	Biot number referring to vapor transport, $\bar{h}_v\bar{L}/\bar{\alpha}_{\text{eff},0}$
$\bar{C}_p$	average heat capacity [W s kg^{-1} K^{-1}]
$\bar{c}_i$	dimensional heat capacity for the ith phase at constant pressure [W s kg^{-1} K^{-1}]
$\bar{c}_0$	reference heat capacity [W s kg^{-1} K^{-1}]
$\bar{D}_{v,\text{eff}}$	effective vapor diffusivity coefficient [m^2 s^{-1}]
$\mathbf{g}$	dimensionless gravity vector
$\bar{h}$	heat transfer coefficient [W m^{-2} K^{-1}]
$\bar{h}^*$	mass transfer coefficient [m s^{-1}]
$\bar{h}_v$	species transfer coefficient [m s^{-1}]
$\Delta\bar{h}_{\text{vap}}$	enthalpy of vaporization per unit mass [J kg^{-1}]
$\bar{H}$	height of the porous insulation [m]
$\bar{H}'$	length of the opening of the porous insulation [m]
$\bar{k}_i$	dimensional thermal conductivity for phase i [W m^{-1} K^{-1}]
$\bar{k}_{\langle\bar{T}\rangle}$	$-\partial\langle\bar{p}_c\rangle/\partial\langle\bar{T}\rangle$ [N m^{-2} K^{-1}]
$\bar{k}_s$	$-\partial\langle\bar{p}_c\rangle/\partial\varepsilon_\beta$ [N m^{-2}]
$\bar{k}_{\text{eff}}$	dimensional effective thermal conductivity [W m^{-1} K^{-1}]
$\bar{K}$	permeability [m^2]
$\bar{K}_\beta$	effective liquid permeability [m^2]
$\bar{K}_\gamma$	effective gas permeability [m^2]
$K_{r\beta}$	relative permeability for the liquid phase
$K_{r\gamma}$	relative permeability for the gas phase
$\bar{L}$	thickness of the insulation [m]
Le	Lewis number, $\bar{\alpha}_{\text{eff},0}/\bar{D}_{v,\text{eff}}$
$\bar{m}$	dimensional condensation rate [kg m^{-3} s^{-1}]
p_a	dimensionless air pressure, $\bar{p}_a/\bar{p}_{a,0}$
$\bar{p}_c$	capillary pressure, $\bar{p}_\gamma-\bar{p}_\beta$ [N m^{-2}]
p_v	dimensionless vapor pressure, $\bar{p}_v/\bar{p}_{v,0}$
p_γ	dimensionless gas phase pressure, $\bar{p}_\gamma/\bar{p}_{\gamma,0}$
Δp_γ	dimensionless gas pressure difference across the insulation, $\Delta\bar{p}_\gamma/\bar{p}_{\gamma,0}$
Pe	Peclet number, $\bar{v}_{\gamma,0}\bar{L}/\bar{\alpha}_{\text{eff},0}$
$\bar{r}$	characteristic length of the porous matrix [m]
$\bar{R}_a$	air gas constant [N m kg^{-1} K^{-1}]
$\bar{R}_v$	vapor gas constant [N m kg^{-1} K^{-1}]
s	scaled fractional liquid saturation, $(s_\beta-s_{\beta p})/(1-s_{\beta p})$
s_β	fractional liquid saturation, $\varepsilon_\beta/(\varepsilon_\beta+\varepsilon_\gamma)$
$s_{\beta p}$	saturation for the immobile liquid
t	dimensionless time, $\bar{t}/(\bar{L}^2/\bar{\alpha}_{\text{eff},0})$
T	dimensionless temperature, $\bar{T}/\Delta\bar{T}$
$\bar{T}_{\infty,h}$	hot-side ambient temperature [K]
$\bar{T}_{\infty,c}$	cool-side ambient temperature [K].

Greek symbols

$\bar{\alpha}_{\text{eff},0}$	reference effective thermal diffusivity, $\bar{k}_{\text{eff},0}/(\bar{\rho}_0\bar{c}_0)$ [m^2 s^{-1}]
ε	volume fraction
η	opening size, $\bar{H}'/\bar{H}$
$\bar{\mu}_\beta$	liquid dynamic viscosity [kg m^{-1} s^{-1}]
$\bar{\mu}_\gamma$	gas dynamic viscosity [kg m^{-1} s^{-1}]
$\bar{\rho}$	dimensional total density defined in equation (16) [kg m^{-3}]
ρ_i	dimensionless density for phase i, $\bar{\rho}_i/\bar{\rho}_{i,0}$
ρ_v	dimensionless vapor density, $\bar{\rho}_v/\bar{\rho}_{v,0}$
$\bar{\sigma}_{\beta\gamma}$	surface tension at the gas and liquid interface [N m^{-1}]
$\omega_{\infty,h}$	hot-side ambient relative humidity
$\omega_{\infty,c}$	cool-side ambient relative humidity.

Subscripts

a	air phase
c	cool side of the insulation
eff	effective properties
h	hot side of the insulation
i	ith phase
s	saturation quantities
v	vapor phase
x	component in the x-direction
β	liquid phase
γ	gas phase
σ	solid matrix
0	reference quantities
∞	ambient quantities in the surroundings.

Superscript

$\bar{}$	dimensional quantities.

Other symbol

$\langle\ \rangle$	'local volume average' of the quantity.

and Tien [21]. Also, Bankvall has worked on several investigations on natural convection and heat transfer through porous insulations [22, 23]. In the present work in addition to including the phase change and multi-component effects, the full compressibility effects were also accounted for, i.e. the Boussinesq approximation was not utilized.

In the present study, attention is given to a more realistic physical system as shown in Fig. 1. The vertical boundaries of the porous insulation are partially permeable to simulate the holes or cracks in walls, which are subjected to the external pressure forces (infiltration). The horizontal boundaries are assumed to be impermeable and insulated. The impermeable

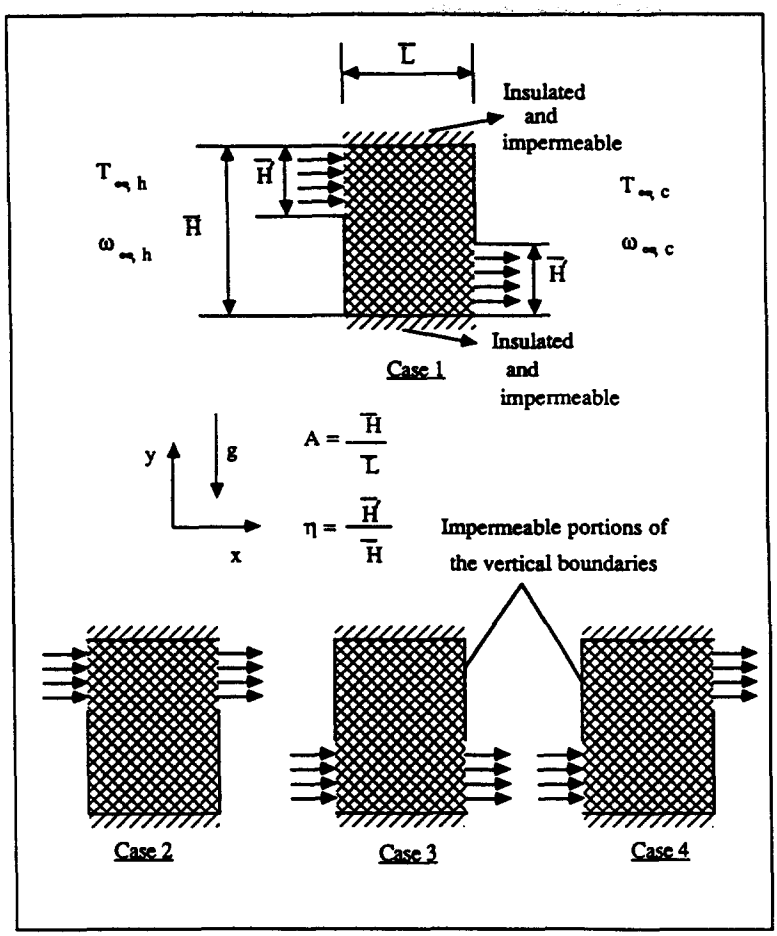

FIG. 1. Schematic diagram of a two-dimensional porous matrix with partially permeable boundaries for four representative opening locations.

parts of the vertical boundaries are also assumed to be insulated. The temperature and vapor density boundary conditions for the permeable parts are not specified; rather, convective boundary conditions are applied. The inter-relationship and variations of the important variables are thoroughly investigated. The effects of the Biot number, opening size, and opening locations are investigated. This study can serve as a significant step towards full simulation of condensation problems with infiltration in porous insulations.

2. ANALYSIS

2.1. *Governing equations*

The governing equations for heat and mass transfer in a porous medium with phase change are derived by using the local volume averaging technique. The derivation of the governing equations is based on the work of Whitaker [4]. The non-dimensional governing equations are found as follows:

thermal energy equation

$$\frac{\partial\langle T\rangle}{\partial t}+\frac{P_1P_2P_{18}}{P_{19}}\psi_\varepsilon\langle \mathbf{v}_\beta\rangle\cdot\nabla\langle T\rangle + \frac{P_3P_4P_{18}\,Pe}{P_{19}}\langle\rho_\gamma\rangle^\gamma\langle \mathbf{v}_\gamma\rangle\cdot\nabla\langle T\rangle+\frac{P_{18}}{P_{19}}\langle\dot{m}\rangle = P_{18}\nabla^2\langle T\rangle+\frac{P_{18}}{P_{19}}\nabla P_{19}\cdot\nabla\langle T\rangle; \quad (1)$$

liquid phase equation of motion

$$\langle \mathbf{v}_\beta\rangle = -K_{r\beta}(\nabla\varepsilon_\beta+\psi_T\nabla\langle T\rangle-\psi_g\mathbf{g}); \quad (2)$$

liquid phase continuity equation

$$\frac{\partial\varepsilon_\beta}{\partial t}+\psi_\varepsilon\nabla\cdot\langle \mathbf{v}_\beta\rangle+\frac{1}{P_1P_6}\langle\dot{m}\rangle=0; \quad (3)$$

gas phase equation of motion

$$\langle \mathbf{v}_\gamma\rangle = P_{20}K_{r\gamma}(-\nabla\langle p_\gamma\rangle^\gamma+P_5\langle\rho_\gamma\rangle^\gamma\mathbf{g}); \quad (4)$$

gas phase continuity equation

$$\frac{\partial}{\partial t}(\varepsilon_\gamma\langle\rho_\gamma\rangle^\gamma)+Pe\,\nabla\cdot(\langle\rho_\gamma\rangle^\gamma\langle\mathbf{v}_\gamma\rangle)-\frac{1}{P_4P_6}\langle\dot{m}\rangle=0; \tag{5}$$

gas phase diffusion equation

$$\frac{\partial}{\partial t}(\varepsilon_\gamma\langle\rho_v\rangle^\gamma)+Pe\,\nabla\cdot(\langle\rho_v\rangle^\gamma\langle\mathbf{v}_\gamma\rangle)-\frac{1}{P_4P_6P_{11}}\langle\dot{m}\rangle=\frac{1}{Le}\nabla\cdot\left[\langle\rho_\gamma\rangle^\gamma\nabla\left(\frac{\langle\rho_v\rangle^\gamma}{\langle\rho_\gamma\rangle^\gamma}\right)\right]; \tag{6}$$

volume constraint

$$\varepsilon_\sigma+\varepsilon_\beta+\varepsilon_\gamma=1; \tag{7}$$

thermodynamic relations

$$\langle p_v\rangle^\gamma=P_9\langle\rho_v\rangle^\gamma\langle T\rangle \tag{8}$$

$$\langle p_a\rangle^\gamma=P_9\langle\rho_a\rangle^\gamma\langle T\rangle \tag{9}$$

$$\langle\rho_\gamma\rangle^\gamma=P_{11}\langle\rho_v\rangle^\gamma+P_{12}\langle\rho_a\rangle^\gamma \tag{10}$$

$$\langle\rho_\gamma\rangle^\gamma=P_{13}\langle p_v\rangle^\gamma+P_{14}\langle p_a\rangle^\gamma \tag{11}$$

$$\langle\rho_{v,s}\rangle^\gamma=\frac{1}{P_9\langle T\rangle}\exp\left(-\frac{P_{15}+P_{16}}{\langle T\rangle}+\frac{P_{16}}{\langle T_0\rangle}\right). \tag{12}$$

The variable properties in the porous insulation are

$$\bar{k}_{\text{eff}}\cong\varepsilon_\sigma\bar{k}_\sigma+\varepsilon_\beta\bar{k}_\beta+\varepsilon_\gamma\frac{(\bar{k}_v\langle\bar{\rho}_v\rangle^\gamma+\bar{k}_a\langle\bar{\rho}_a\rangle^\gamma)}{(\langle\bar{\rho}_v\rangle^\gamma+\langle\bar{\rho}_a\rangle^\gamma)} \tag{13}$$

$$\bar{\rho}=\varepsilon_\sigma\bar{\rho}_\sigma+\varepsilon_\beta\bar{\rho}_\beta+\varepsilon_\gamma(\langle\bar{\rho}_v\rangle^\gamma+\langle\bar{\rho}_a\rangle^\gamma) \tag{14}$$

$$\bar{C}_p=\frac{\varepsilon_\sigma\bar{\rho}_\sigma\bar{c}_\sigma+\varepsilon_\beta\bar{\rho}_\beta\bar{c}_\beta+\varepsilon_\gamma(\langle\bar{\rho}_v\rangle^\gamma\bar{c}_v+\langle\bar{\rho}_a\rangle^\gamma\bar{c}_a)}{\bar{\rho}} \tag{15}$$

$$\bar{\alpha}_{\text{eff}}=\frac{\bar{k}_{\text{eff}}}{\bar{\rho}\bar{C}_p}. \tag{16}$$

In the above equations, the main variables of interest are the temperature T, the liquid volume fraction ε_β, the vapor density ρ_v, the gas density ρ_γ, the gas volume fraction ε_γ, and the condensation rate $\dot{m}$. The variables with a bar over them refer to dimensional quantities. The dimensionless variables and nondimensional parameters Pe, Le, ψ_ε, ψ_g, ψ_T and P_j's, are defined in the Appendix. It should be mentioned that in the above equations, $\langle\Psi\rangle$ is the spatial average for a quantity Ψ and is defined as

$$\langle\Psi\rangle=\frac{1}{V}\int_V\Psi\,dV \tag{17}$$

where V is an averaging volume which is bounded by a closed surface in the porous medium. The averaging volume V is composed of three phases, the solid phase V_σ, the liquid phase $V_\beta(t)$, and the gas phase $V_\gamma(t)$. Another averaging quantity in the governing equations is the intrinsic phase average which is given by

$$\langle\Psi_\alpha\rangle^\alpha=\frac{1}{V_\alpha(t)}\int_{V_\alpha(t)}\Psi\,dV \tag{18}$$

where Ψ_α is a quantity associated with the α phase.

In arriving at the governing equations, only three major assumptions were made:

(1) the porous insulation material is homogeneous and isotropic;

(2) the three phases in the porous system are assumed to be in local thermodynamic equilibrium;

(3) Darcy's flow model is valid in describing the motion of the gas phase and the liquid phase.

The first two assumptions are the common simplifying procedure to rationally tackle the problems for heat and mass transport in porous materials. The third assumption is justified due to the following reasons. Vasseur *et al.* [24] used the results of ref. [25] to examine the validity of Darcy's law. Based on their results, two conditions which respectively characterize the inertia and the boundary effects, should be satisfied if the results obtained from Darcy's law are to be within a 10% error band. These two conditions are

$$\bar{U}<\frac{6\times10^{-3}\,\bar{\nu}}{(1-\varepsilon_\sigma)F\sqrt{\bar{K}}}\quad\text{and}\quad\bar{L}>Pr\sqrt{(\bar{K}/(1-\varepsilon_\sigma))} \tag{19}$$

where $\bar{U}$ is the characteristic fluid velocity, $\bar{\nu}$ the kinematic viscosity, $(1-\varepsilon_\sigma)$ the porosity, F a coefficient related to the inertia parameter, $\bar{K}$ the permeability, $\bar{L}$ the characteristic length of the porous material, and Pr the Prandtl number. Based on the typical thermophysical data for porous insulations and in this work, these two conditions are apparently satisfied. The dispersion effects are also neglected in this study. Aside from these assumptions, the governing equations are very general and can be applied to a general class of problems for heat and mass transfer in porous materials.

It is noted that the effective gas permeability $\bar{K}_\gamma$ and the effective liquid permeability for partially liquid saturated media $\bar{K}_\beta$ can be expressed in terms of the permeability $\bar{K}$ and the relative permeabilities, $K_{r\beta}$ and $K_{r\gamma}$, as

$$\bar{K}_\gamma=K_{r\gamma}\bar{K}$$

$$\bar{K}_\beta=K_{r\beta}\bar{K}. \tag{20}$$

Based on the relative permeability model suggested by Wyllie [26], which agrees well with the data in the work of Fatt and Klikoff [27] and is also used by Udell [10], the relative permeabilities are taken to have the following forms:

$$K_{r\beta}=s^3$$

$$K_{r\gamma}=(1-s)^3 \tag{21}$$

where

$$s = \frac{s_\beta - s_{\beta p}}{1 - s_{\beta p}} \quad \text{and} \quad s_\beta = \frac{\varepsilon_\beta}{\varepsilon_\beta + \varepsilon_\gamma}. \tag{22}$$

The variable $s_{\beta p}$ is the saturation of the liquid in pendular state in the porous medium. Below this saturation, the liquid is essentially immobile due to no inter-pore connections. There were no concrete experimental data available for $s_{\beta p}$, however a value of 0.1 was found to be a reasonable one. This value was also used by Kaviany and Mittal [8].

2.2. *Boundary conditions*

As mentioned earlier, in our investigation the horizontal boundaries are chosen to be insulated and impermeable while the vertical boundaries are only partially insulated and partially impermeable. Convective boundary conditions at the porous medium–surrounding gas interface are formulated as in the work of Whitaker [4]. The non-dimensional boundary conditions for the mass, energy and species balance are found as follows:

mass balance

$$(P_1 \psi_\varepsilon \langle \mathbf{v}_\beta \rangle + Pe\, P_4 \langle \rho_\gamma \rangle^\gamma \langle \mathbf{v}_\gamma \rangle) \cdot \mathbf{n} = B^* P_4 (\langle \rho_\gamma \rangle^\gamma - \rho_\infty); \tag{23}$$

energy balance

$$P_1 P_6 \psi_\varepsilon \langle \mathbf{v}_\beta \rangle \cdot \mathbf{n} + P_{19} \nabla T \cdot \mathbf{n} = B(T_\infty - \langle T \rangle); \tag{24}$$

species balance

$$\left[P_1 \psi_\varepsilon \langle \mathbf{v}_\beta \rangle + Pe\, P_4 P_{11} \langle \rho_v \rangle^\gamma \langle \mathbf{v}_\gamma \rangle - \frac{P_4 P_{11}}{Le} \langle \rho_\gamma \rangle^\gamma \nabla \left(\frac{\langle \rho_v \rangle^\gamma}{\langle \rho_\gamma \rangle^\gamma} \right) \right] \cdot \mathbf{n} = B_v P_4 P_{11} (\langle \rho_v \rangle^\gamma - \rho_{v,\infty}) \tag{25}$$

where $\mathbf{n}$ is the unit normal vector which points out from the porous medium into the surrounding gas phase, and B^*, B and B_v are the Biot numbers referring to, the mass transfer, heat transfer, and species transport, respectively. For the permeable portions of the vertical boundaries, B and B_v are nonzero. However, for the impermeable portions of the vertical boundaries as well as the horizontal boundaries, B and B_v are both set to zero. The pressures are specified at the permeable parts of the vertical boundaries as

$$p_\gamma(x = 0, y, t) = 1 + \Delta p_\gamma$$
$$p_\gamma(x = 1, y, t) = 1 \tag{26}$$

where Δp_γ denotes the non-dimensional pressure difference across the insulation. In this study Δp_γ is taken as 10^{-5}, except for the results which are presented in Table 3 and are discussed later on, to simulate the real situation for which the pressure differences are very small. The ambient conditions are

$$T_{\infty,h} = 15.4$$
$$T_{\infty,c} = 14.65 \tag{27}$$

and

$$\omega_{\infty,h} = 1$$
$$\omega_{\infty,c} = 1. \tag{28}$$

The initial conditions are specified as

$$T(x, y, t = 0) = 14.65$$
$$\omega(x, y, t = 0) = 1$$
$$\varepsilon_\beta(x, y, t = 0) = 0$$
$$p_\gamma(x, y, t = 0) = 1. \tag{29}$$

It should be noted that the above non-dimensional ambient temperatures translate into $\bar{T}_{\infty,h} = 308$ K and $\bar{T}_{\infty,c} = 293$ K which are based on physical grounds.

2.3. *Heat transfer calculation*

The overall heat transfer across the porous insulation, which includes both the heat and mass transfer, is best characterized by the average Nusselt number for each permeable portion of the walls. The Nusselt number at the hot side, Nu_h, is defined as

$$Nu_h = \frac{1}{\eta A} \frac{\int_y^{y+\eta A} \left(-P_{19} \frac{\partial T}{\partial x} + P_3 P_4\, Pe\, \rho_\gamma v_{\gamma_x} T + P_1 P_2 \psi_\varepsilon v_{\beta_x} T \right)\Big|_{x=0} \mathrm{d}y}{P_{19}(T_{\infty,h} - T_{\infty,c}) + P_3 P_4\, Pe\, \rho_\gamma^* v_{\gamma_x}^* T_{\infty,h}}. \tag{30}$$

The Nusselt number, as defined in equation (30), accounts for the contribution of heat conduction, infiltration and bulk convection. In the above expression, the numerator accounts for the actual heat transfer and the denominator represents a suitable chosen reference heat transfer. It should be noted that the integration in the numerator is carried out over the permeable area only. Since, as will be seen later, the major contribution to the overall heat transfer is due to infiltration, it is then reasonable to include the infiltration effect in the reference heat flux which is used to form the Nusselt number. For this reason, the second term in the denominator on the right-hand side of equation (30) accounts for a one-dimensional infiltration. Also, η is the opening size, which is the ratio of the area of the opening to the total area of the vertical boundary.

2.4. *Physical data*

Table 1 displays all the physical data used in our computational experiments. These data are based on the typical properties for the gas, liquid and the solid phases. It should be noted that although the Kelvin

Table 1. Physical data

(a) Reference quantities

$\bar{\rho}_0$ (kg m^{-3})	$\bar{c}_0$ (J kg^{-1} K^{-1})	$\bar{\rho}_{v,0}$ (kg m^{-3})	$\bar{\rho}_{a,0}$ (kg m^{-3})	$\bar{\rho}_{\gamma,0}$ (kg m^{-3})	$\bar{T}_0$ (K)	$\bar{p}_{\gamma,0}$ (N m^{-2})	$\bar{k}_{eff,0}$ (W m^{-1} K^{-1})
76.89	842	0.03966	1.08216	1.12182	308	1.013×10^5	0.026

(b) Solid phase

ε_σ	L (m)	$\bar{\rho}_\sigma$ (kg m^{-3})	$\bar{c}_\sigma$ (J kg^{-1} K^{-1})	$\bar{k}_\sigma$ (W m^{-1} K^{-1})
0.03	0.12	2563	835	0.043

(c) Liquid phase

$\bar{\rho}_\beta$ (kg m^{-3})	$\bar{c}_\beta$ (J kg^{-1} K^{-1})	$\bar{k}_\beta$ (W m^{-1} K^{-1})	$\bar{\mu}_\beta$ (kg m^{-1} s^{-1})
1000	4182	0.603	0.8×10^{-3}

(d) Gas phase

$\bar{c}_v$ (J kg^{-1} K^{-1})	$\bar{c}_a$ (J kg^{-1} K^{-1})	$\bar{k}_v$ (W m^{-1} K^{-1})	$\bar{k}_a$ (W m^{-1} K^{-1})	$\bar{R}_v$ (J kg^{-1} K^{-1})	$\bar{R}_a$ (J kg^{-1} K^{-1})	$\bar{\mu}_\gamma$ (kg m^{-1} s^{-1})
1866	1000	0.0191	0.0262	462	287	1.846×10^{-5}

(e) Other quantities

K (m^2)	$\bar{D}_{v,eff}$ (m^2 s^{-1})	$\Delta\bar{T}$ (K)	$\Delta\bar{h}_{vap}$ (J kg^{-1})	$\bar{\sigma}_{\beta\gamma}$ (kg s^{-2})
7.25×10^{-10}	2.8×10^{-5}	20	2.4425×10^6	0.07

effect has been taken into account in equation (12), a surface tension of 0.07 kg m^{-2} translates into $P_{15} \ll P_{16}$ if $O(\bar{r}) > 10^{-9}$ m. This fact was also given in the work of Whitaker and Chou [7], where it was mentioned that surface tension had very little effect on the saturation vapor pressure.

3. METHOD OF SOLUTION

The complete system of equations along with the boundary conditions were solved by an efficient finite difference scheme. In this scheme, the spatial derivatives were discretized by the central differencing except for most of the convective terms which were approximated by the first-order upwind differencing. The numerical scheme consists of two different formats which had the capability of accounting for phase change. For $\varepsilon_\beta < 10^{-5}$, the liquid content was considered to be part of the adsorbed water; therefore, no bulk condensation was possible and the condensation rate was set equal to zero. When the liquid content is greater than 10^{-5}, condensation was taken into account. Further details on the two phase format can be found in ref. [19].

Two checks were made in order to investigate the accuracy of the scheme. First, the effect of the time step size was checked by fixing the grid size while varying the time step size. It was found that decreasing the time step size beyond a certain value which was used in the numerical experiments did not have an effect on the heat transfer results and the distributions of the field variables. Next, a comparison of the Nusselt number results was made using three different grid systems, given by 11×11, 15×15 and 21×21 as shown in Table 2. As can be seen from the results given in Table 2, a very good agreement exists between 15×15 and 21×21 results. It should be mentioned that the CPU time becomes very excessive for the 21×21 grid system. The intensive CPU time which is required for this problem is due to the intercoupled and complicated nature of the problem, which dictates the use of a very small time step size. In order to conserve the CPU time, the 15×15 grid system is used for most of the runs.

Table 2. Effect of the grid size on the Nusselt number

t	Nu_h (11 × 11)	Relative difference between (11 × 11) and (21 × 21) grid systems (%)	Nu_h (15 × 15)	Relative difference between (15 × 15) and (21 × 21) grid systems (%)	Nu_h (21 × 21)
0.0005	2.4896	1.54	2.5444	0.63	2.5285
0.001	2.4009	1.00	2.4191	0.25	2.4252
0.0015	2.3488	0.71	2.3732	0.33	2.3655
0.002	2.3092	1.10	2.3360	0.04	2.3350
0.0025	2.2943	0.74	2.3130	0.07	2.3114
0.003	2.2788	0.64	2.2955	0.09	2.2934
0.0035	2.2640	0.78	2.2845	0.12	2.2818
0.004	2.2520	0.79	2.2740	0.18	2.2699
0.0045	2.2446	0.72	2.2646	0.17	2.2608
0.005	2.2356	0.76	2.2568	0.18	2.2527

Note: Relative difference $\equiv \dfrac{|Nu_{h,21\times21} - Nu_{h,11\times11 \text{ or } 15\times15}|}{Nu_{h,21\times21}}$.

4. RESULTS AND DISCUSSION

As mentioned earlier, the objective of this study is to investigate the dynamic response and thermal behavior of porous materials with partially permeable boundaries which are subjected to specified pressure gradient and convective boundary conditions. The interaction between the field variables is demonstrated. In addition, the effects of the Biot numbers, B's and B_v's, the area and the locations of the openings are investigated. Four fundamental cases are analyzed in this work. These four configurations are represented in Fig. 1. The results, shown in Figs. 2–14, are based on the case with the openings on the upper

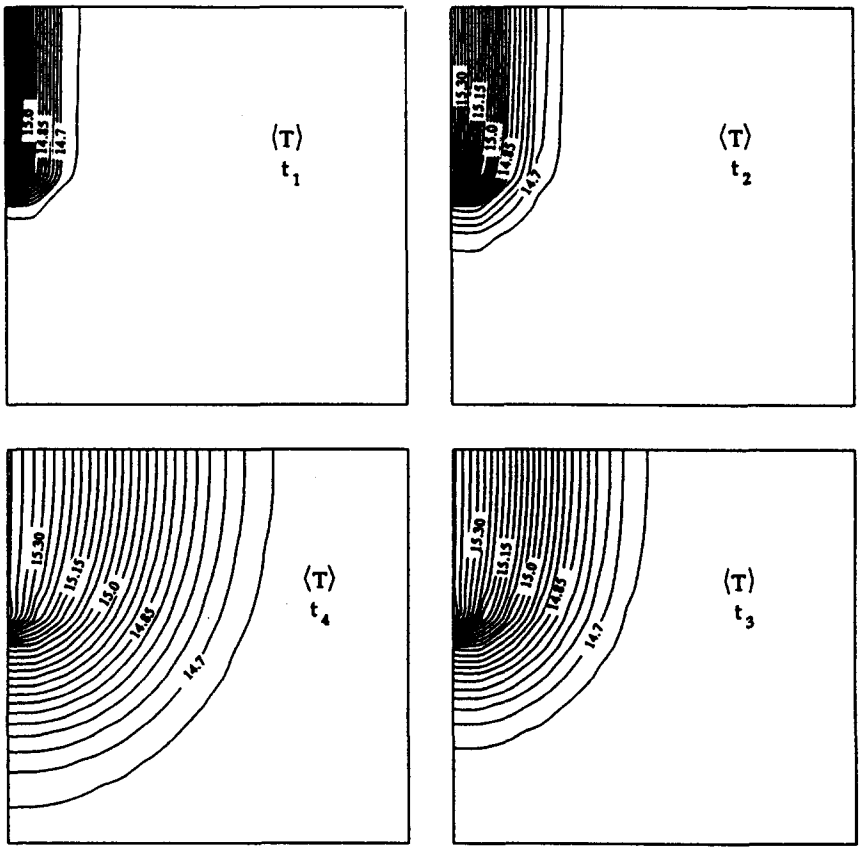

FIG. 2. Spatial variation of temperature inside the porous material for $B = 1000$, $B_v = 5 \times 10^4$ and opening size of 1/2 at four different times: $t_1 = 0.0005$, $t_2 = 0.0015$, $t_3 = 0.005$, $t_4 = 0.01$.

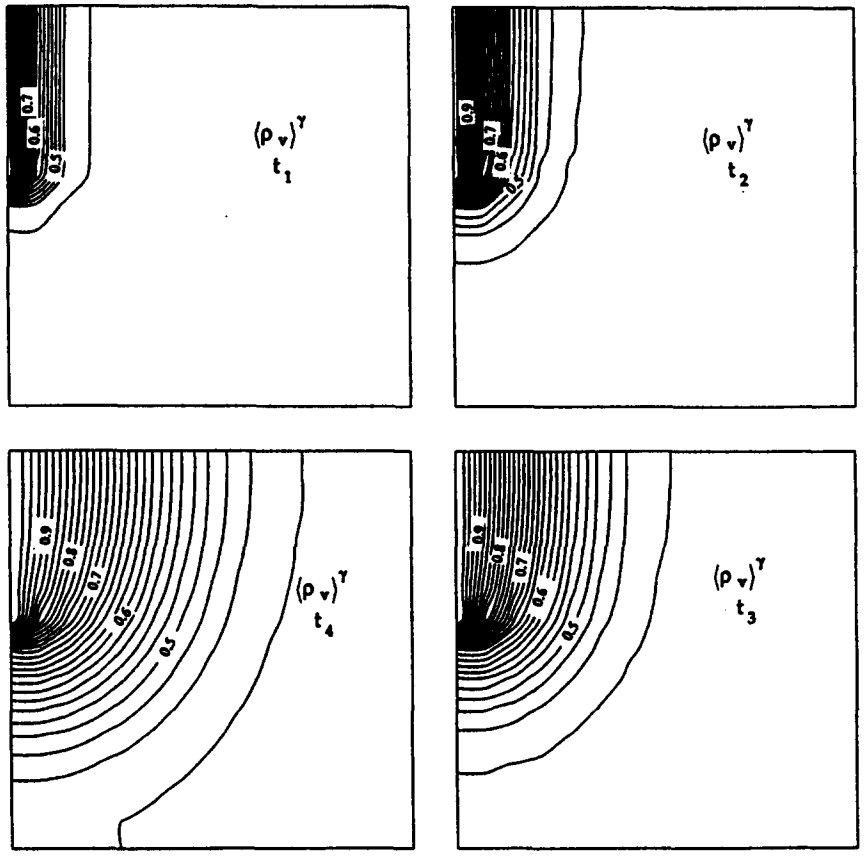

FIG. 3. Vapour density distributions for $B = 1000$, $B_v = 5 \times 10^4$ and an opening size of 1/2, at four different times corresponding to Fig. 2.

left-hand side and lower right-hand side of boundaries, respectively, case (1) in Fig. 1.

Figures 2–5 illustrate the spatial and temporal distributions for the temperature, vapor density, condensation rate and the liquid content. As can be seen in Fig. 2, when the boundaries of the porous system are suddenly exposed to the ambient conditions, the left boundary which is next to the hot and humid environment experiences a sudden increase in temperature. This temperature increase then propagates into the interior region of the porous material at later times. The heat transfer process results from heat conduction, convection, and condensation which acts as a local heat source. The *wave-like* propagating behavior seen in Fig. 2 was also observed for the other variables, such as the vapor density, condensation rate and the liquid content shown in Figs. 3–5. For the sake of brevity, the gas density distributions are not presented here. It should be mentioned that the selected four different times, t_1, t_2, t_3, and t_4 in Figs. 2–5 were chosen so as to characterize the significant variations of the field variables. In all of the figures for the condensation rate, a positive value of $\langle \dot{m} \rangle$ corresponds to condensation whereas a negative value corresponds to evaporation. It should be noted that, as seen in Fig. 5, there is a larger concentration of the liquid at the left boundary which is exposed to the hot and humid environment. The velocity field distribution for this case is depicted in Fig. 14(a). The velocity distribution is presented at time t_3 only since the velocity distributions at other times are quite similar to each other. As can be seen from this figure, the fluid flow starts from the upper left opening, moves towards the interior region and finally flows out of the porous system through the lower right opening. No circulation is observed inside the enclosure. This is because the gas phase velocity is only of the order of 10^{-4}—10^{-3} m s^{-1}. Although the average infiltration velocity is quite small, as will be shown later, it still has a dominant effect on the overall heat transfer.

4.1. *Effects of the convective heat transfer boundary conditions*

To examine the effects of the convective heat transfer boundary conditions on the distributions for the field variables as well as on the Nusselt number, the effects of changes in the Biot number, B, were investigated. This was done for $B = 10$, 100 and 1000 while keeping other parameters fixed. For brevity, the results for $B = 100$ are not presented here. Figures 6–

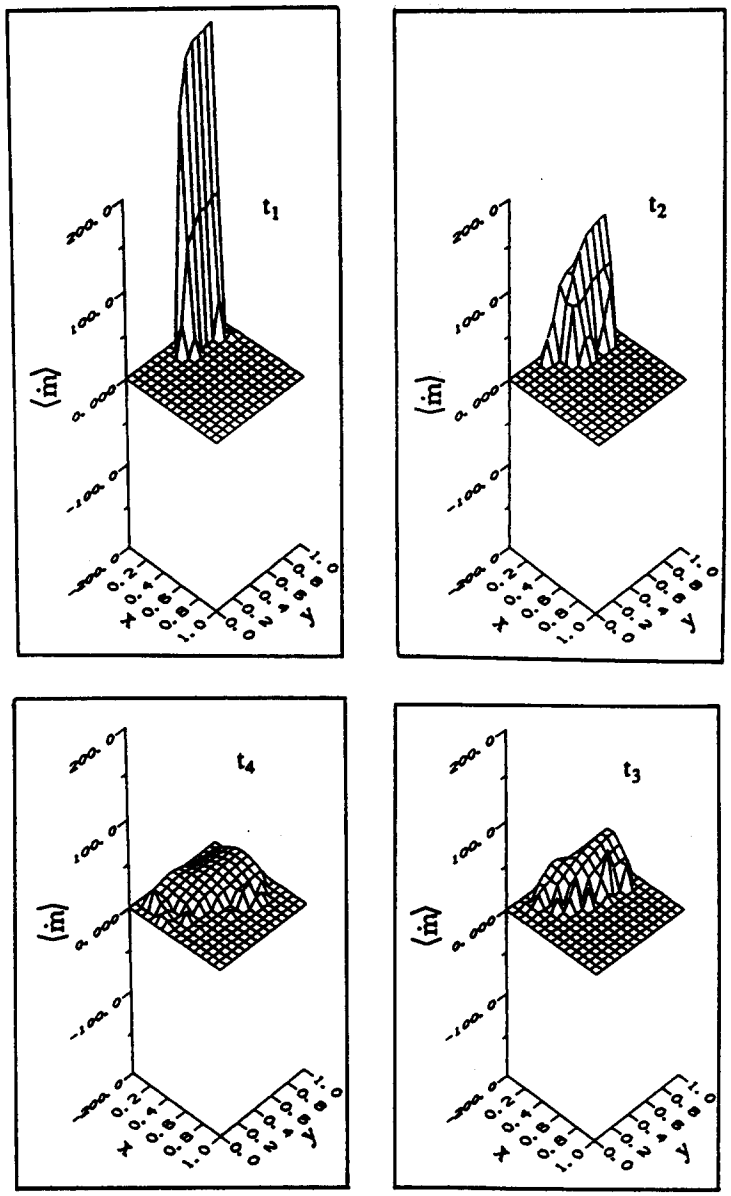

FIG. 4. Three-dimensional condensation rate plots for $B = 1000$, $B_v = 5 \times 10^4$ and an opening size of 1/2 at four different times corresponding to Fig. 2.

9 depict the distributions for the temperature, vapor density, condensation rate and the liquid content for $B = 10$. Comparing Figs. 6–9 with Figs. 2–5 shows that an increase in the Biot number, B, causes an increase in the energy transfer and as a result, enhances the temperature penetration. However, the vapor density distributions are not altered significantly since B_v is kept constant. As a result, the condensation rate is decreased with an increase in the Biot number since the saturation vapor density is mainly dependent on the temperature. Subsequently, the trend for the liquid content follows that of the condensation rate.

The effects of the Biot number on heat transfer results are illustrated in Fig. 10. As expected, as the Biot number increases from 10 to 100 and then 1000, the Nusselt number keeps on increasing. It should be noted that for two orders of magnitude increase in the Biot number, the Nusselt number increases only about 2%. This is because the infiltration is the dominant mode in the overall heat transfer. Therefore, changes in Biot number do not present a significant effect on the Nusselt number.

4.2. *Effects of the convective mass transfer boundary conditions*

To examine the effects of the convective mass transfer boundary conditions, the effects of changes in the

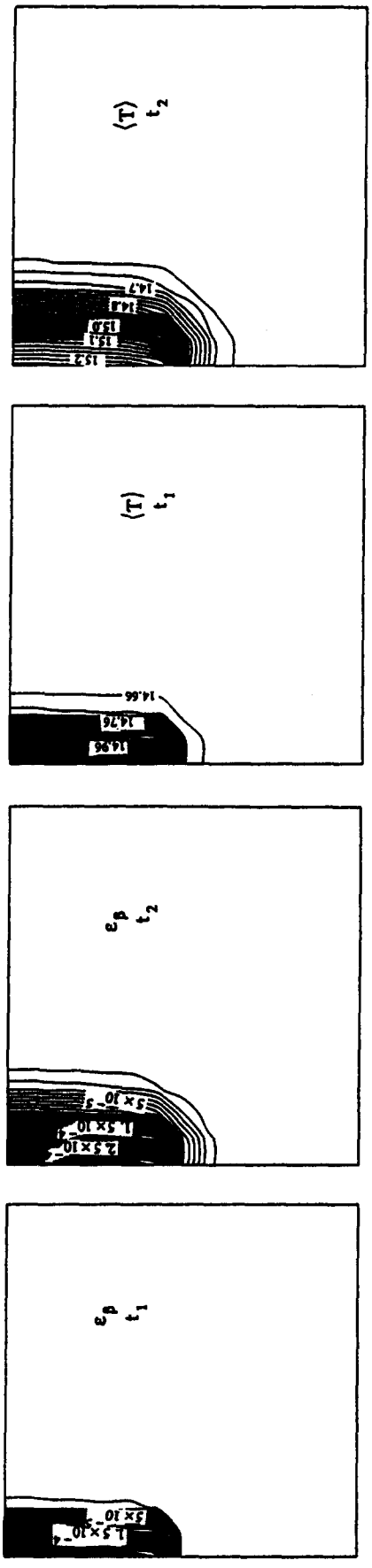

FIG. 5. Liquid content distributions at four different times, corresponding to Fig. 2, for $B = 1000$, $B_r = 5 \times 10^4$ and an opening size of 1/2.

FIG. 6. Spatial variation of temperature inside the porous material for $B = 10$, $B_r = 5 \times 10^4$ and an opening size of 1/2 at four different times corresponding to Fig. 2.

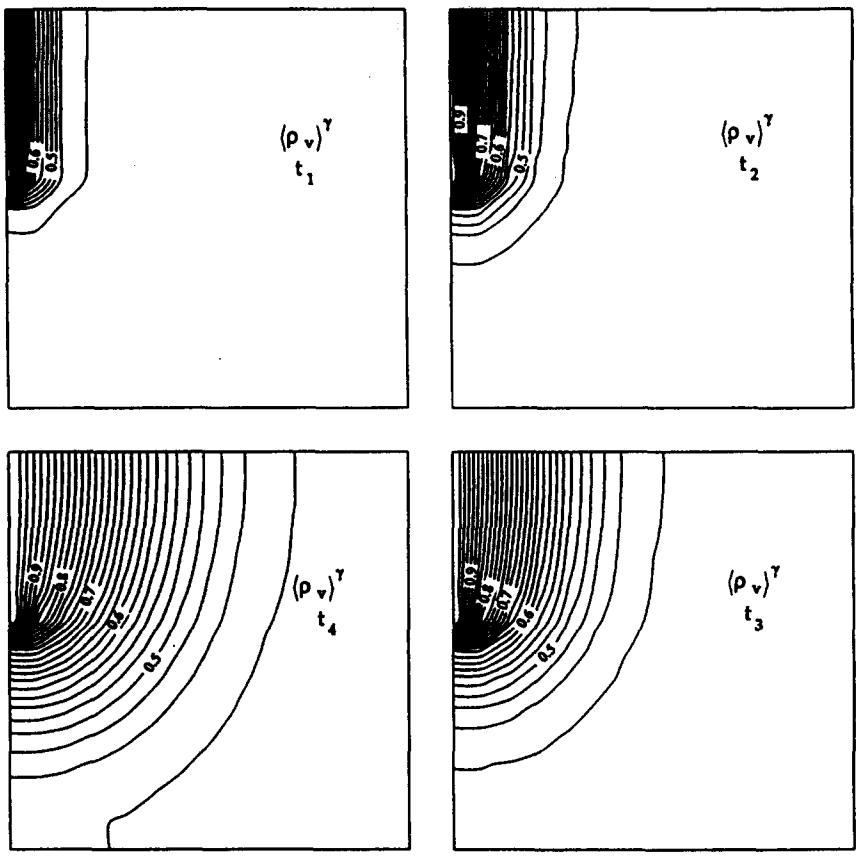

FIG. 7. Vapor density distributions for $B = 10$, $B_v = 5 \times 10^4$ and an opening size of 1/2, at four different times corresponding to Fig. 2.

mass transfer Biot number, B_v, were examined. Figure 11 presents the Nusselt number results for two different B_v's; $B_v = 5 \times 10^4$ and 5×10^3. It is observed that at the initial stage, the Nusselt number for the case with higher B_v is greater than the Nusselt number for the case with lower B_v, while the reverse trend is true at the later stage. This is because initially, the condensation rates close to the left boundary are significantly higher for $B_v = 5 \times 10^4$ than for 5×10^3. However, at later times the temperature next to the hot side increases more rapidly for $B_v = 5 \times 10^4$ than for 5×10^3. Therefore, the temperature gradient at the hot side for the case with larger B_v becomes smaller than the case with smaller B_v at the later stage. As for the effect of B_v on the other field variables, it is found that increasing B_v will enhance the vapor transport, and the liquid content. For brevity, only the condensation rates for the case of $B_v = 5 \times 10^3$ and $B = 1000$ are presented in Fig. 12. The above-mentioned results clearly indicate the complex intercoupled nature of heat transfer and vapor transport in these types of problems.

4.3. *The effects of the permeable region*

A number of interesting results are obtained through the examination of the effects of the opening area on the field variables and the Nusselt number. Figure 13 illustrates the Nusselt number results for two different opening areas, 1/4 and 1/2, with $B = 1000$, $B_v = 5 \times 10^4$. The Nusselt number is significantly higher for the case with smaller opening than the case with larger opening. This is because the case with smaller opening will produce a larger average flow velocity than the case with larger opening, as shown in Fig. 14. It should be noted that the Nusselt number defined in equation (30) is based on the averaged heat transfer along the permeable area of the boundary. So even though the 'averaged' heat transfer rate decreases as the opening increases, the total heat transfer rate will still increase since the heat and mass transfer area increases. This can be seen quite clearly by observing the other two curves in Fig. 13 which are based on the total area of the vertical boundary. It should be mentioned that the Nusselt number defined in equation (30) can always be converted to the one which is based on the total area of the boundary quite easily. This is done by multiplying the Nusselt number by η which is the ratio of the opening area to the total area of the vertical boundary. The distributions for the field variables are qualitatively similar to the previous results and hence they are not presented here.

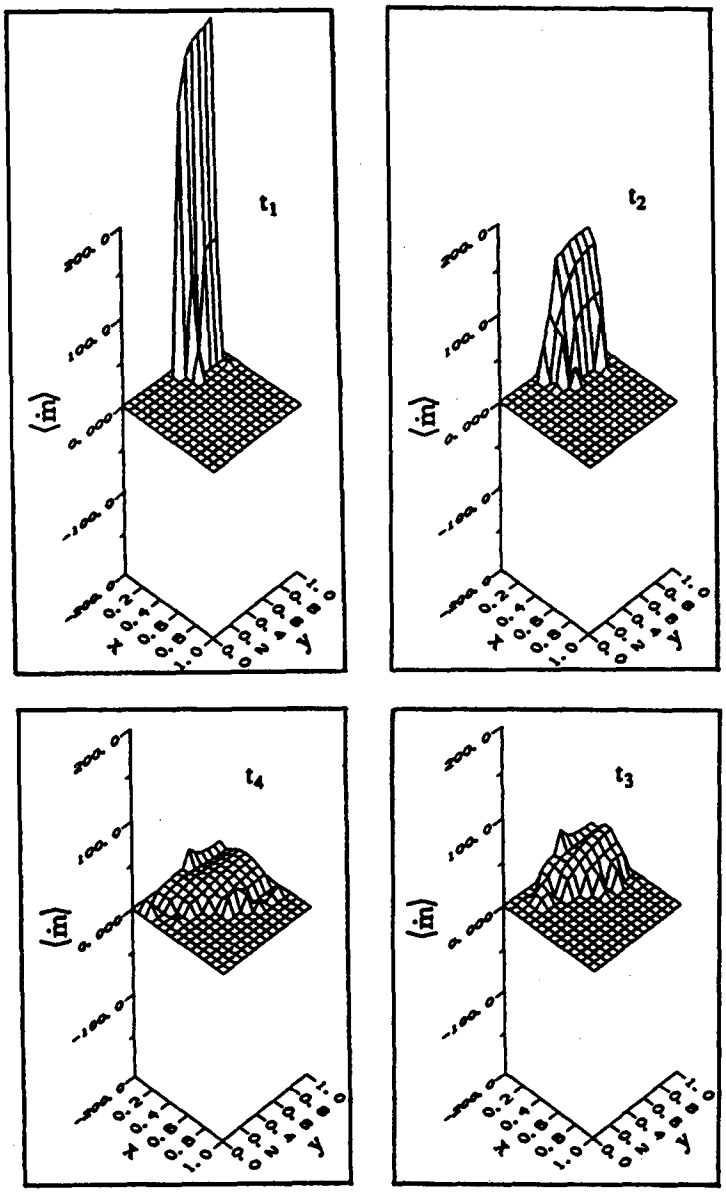

FIG. 8. Three-dimensional condensation rate plots for $B = 10$, $B_v = 5 \times 10^4$ and an opening size of 1/2, at four different times corresponding to Fig. 2.

4.4. The effects of the opening locations, cases 1–4

Figure 1 illustrates the four representative configurations which were discussed earlier. Even though these four cases do not represent all possible combinations, they do present the basic combinations that can exist with respect to the opening locations. An investigation of these different opening locations will therefore provide valuable qualitative information in the design of building insulation configurations.

Figure 15 depicts the Nusselt number results for the aforementioned four configurations with the other parameters, i.e. $B = 1000$, $B_v = 5 \times 10^4$ and an opening size of 1/4, being fixed. Clearly, case 1 gives the highest Nusselt number while case 4 gives the lowest. The Nusselt numbers for cases 2 and 3 are in between and almost equal. The difference in the Nusselt numbers for the four cases can be best explained from the gas velocity distributions which are given in Fig. 16, since the dominant mode of the overall heat transfer is due to infiltration. In case 1, the gravitational force enhances the flow while in case 4 the reverse effect is true. Cases 2 and 3 are in between. In particular, it should be noted that the flow field for case 4 in Fig. 16 is not only quantitatively but qualitatively different from the other cases. This is due to the relatively weak pressure gradient which interacts with the gravitational force and depresses the fluid flow. As a result, the Nusselt number for case 4 as seen in Fig. 15, is

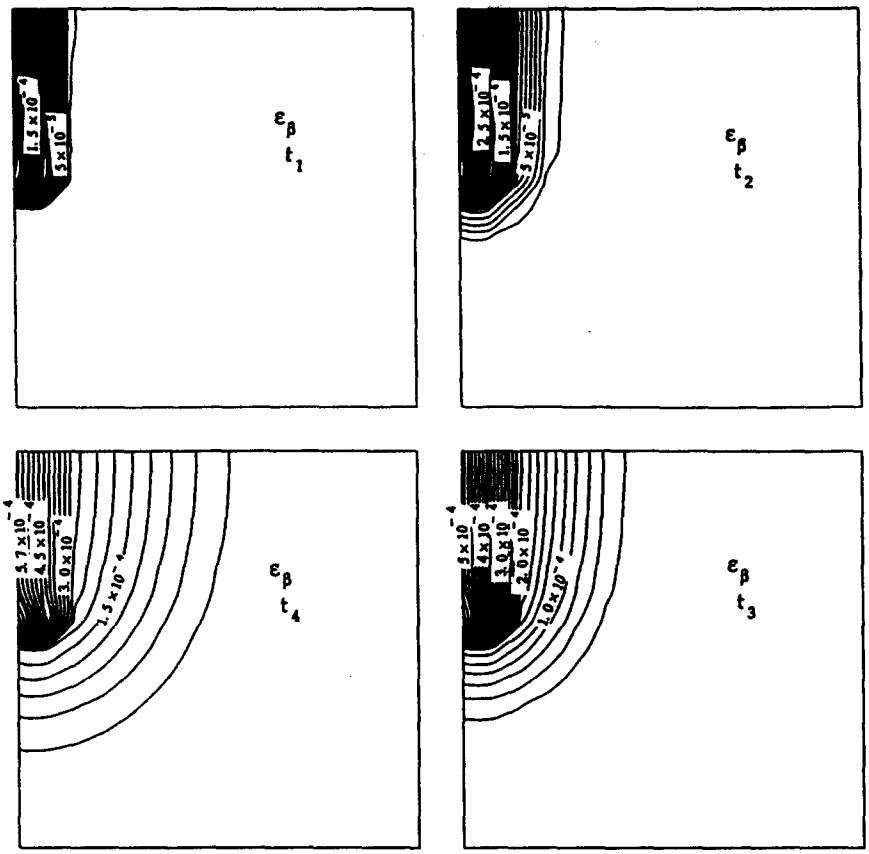

FIG. 9. Liquid content distributions at four different times, corresponding to Fig. 2, for $B = 10$, $B_v = 5 \times 10^4$ and an opening size of 1/2.

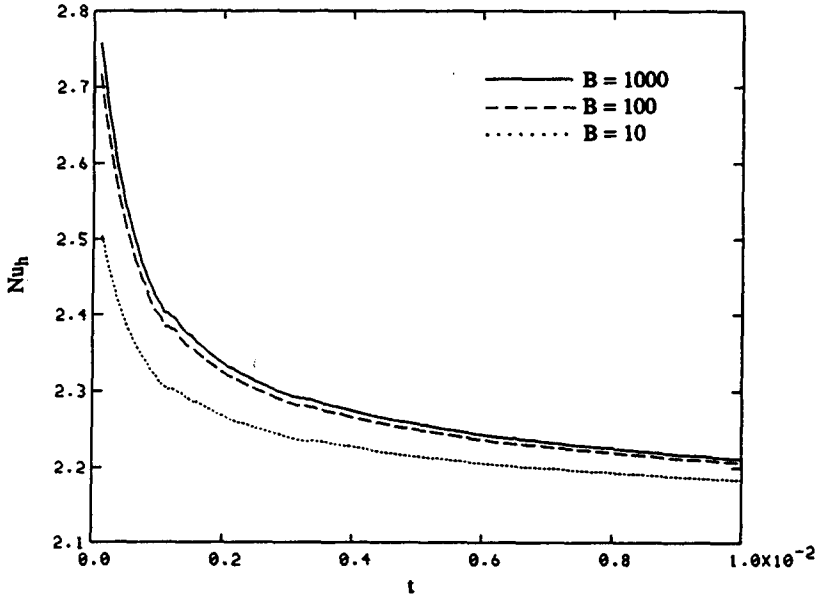

FIG. 10. Effects of the heat transfer Biot number, B, on the Nusselt number for $B_v = 5 \times 10^4$ and an opening size of 1/2.

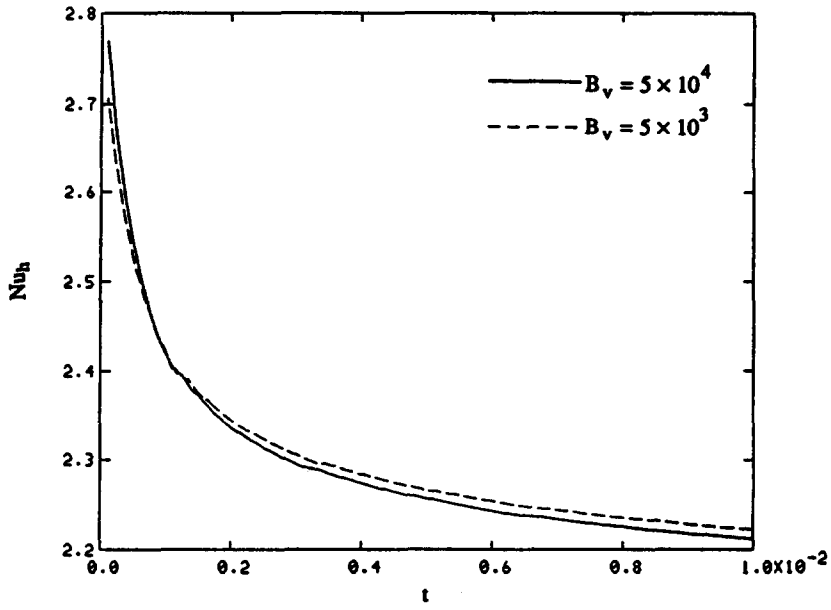

FIG. 11. Effects of the mass transfer Biot number, B_v, on the Nusselt number for $B = 1000$ and an opening size of 1/2.

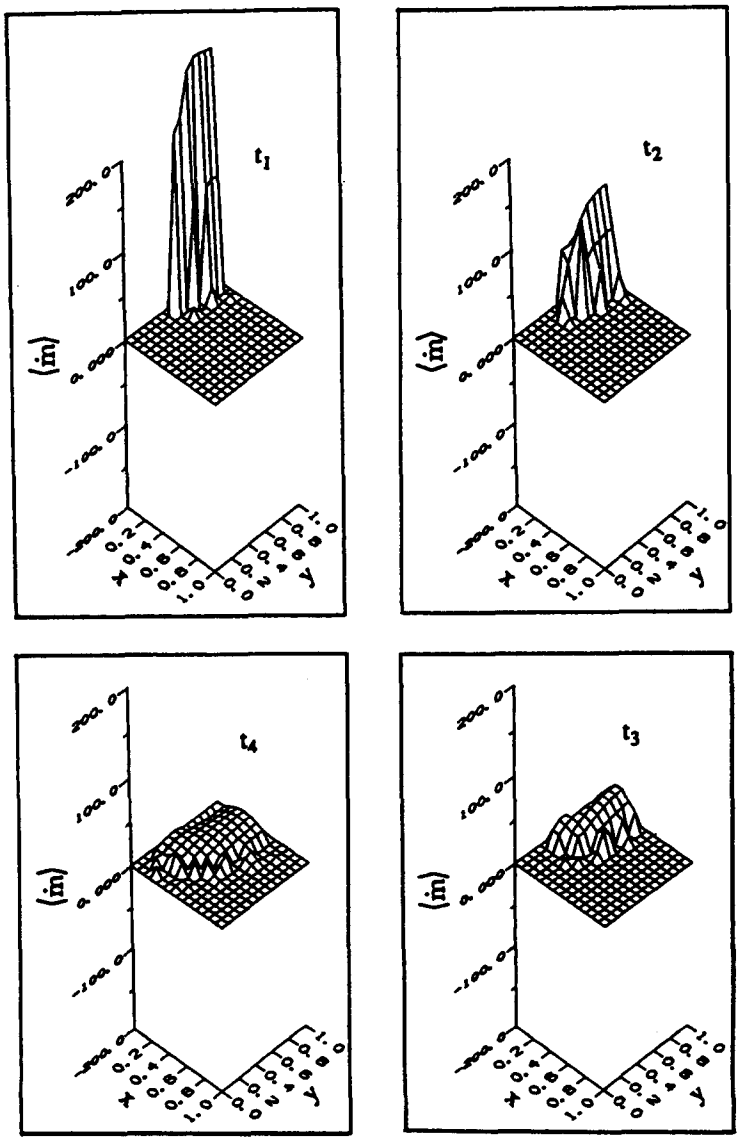

FIG. 12. Three-dimensional condensation rate plots for $B = 1000$, $B_v = 5 \times 10^3$ and an opening size of 1/2, at four different times corresponding to Fig. 2.

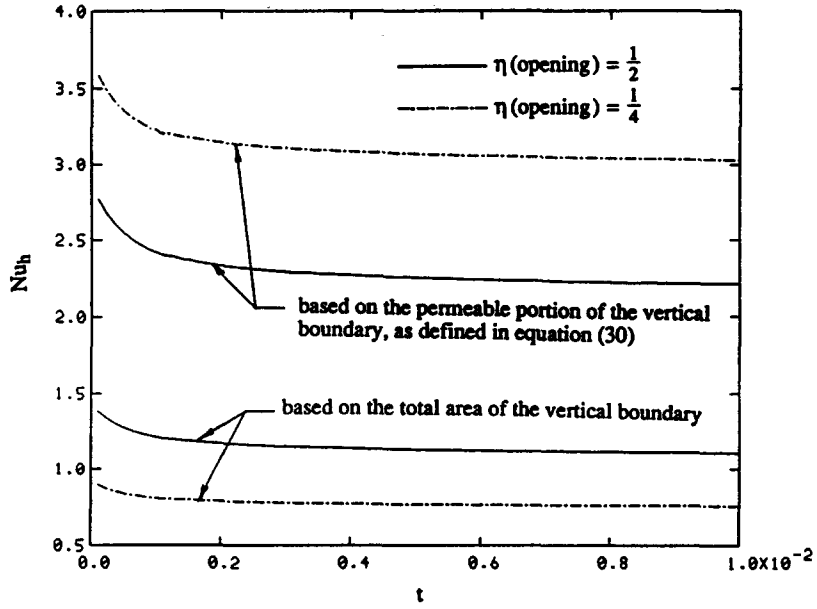

FIG. 13. Effects of the opening size on the Nusselt number for $B = 1000$ and $B_v = 5 \times 10^4$.

less than one. However, it should be noted that the Nusselt number in this work is not defined in the usual way. The effect of one-dimensional uniform infiltration has been included in the reference heat flux which is used in defining the Nusselt number. If the Nusselt number were defined in the usual way, the Nusselt number for case 4 would be greater than one (with one corresponding to pure conduction). The effects of the opening locations on the field variables follow a trend similar to that of Nusselt numbers. The above results make it amply clear that the crack or hole locations in a building have a very significant effect on the heat transfer results as well as the generated liquid condensation.

4.5. *The effects of the pressure difference*, Δp_t

Finally, the effects of the pressure difference Δp_t on the heat and mass transfer through a porous insulation were investigated by increasing Δp_t from 10^{-5} to 10^{-4} and finally to 10^{-3}. The Nusselt number results for these three pressure differences are presented in Table 3 for case 1, with $B = 1000$, $B_v = 5 \times 10^4$ and an opening size ratio of 1/2. As expected, an increase in the pressure difference causes

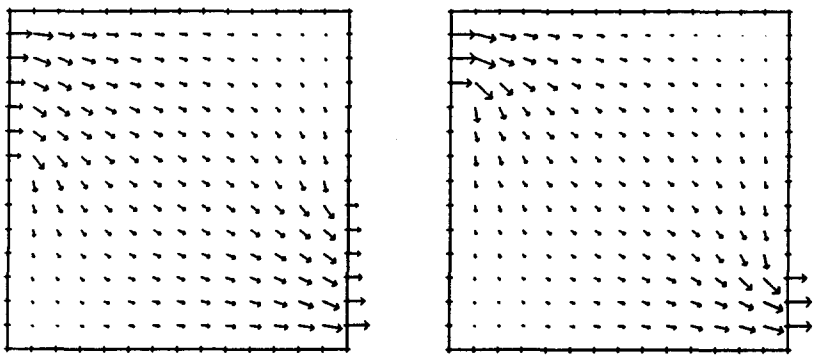

(a) η(opening) = $\frac{1}{2}$ (b) η(opening) = $\frac{1}{4}$

FIG. 14. Effects of the opening size on the gas velocity distributions at t_3 for $B = 1000$ and $B_v = 5 \times 10^4$.

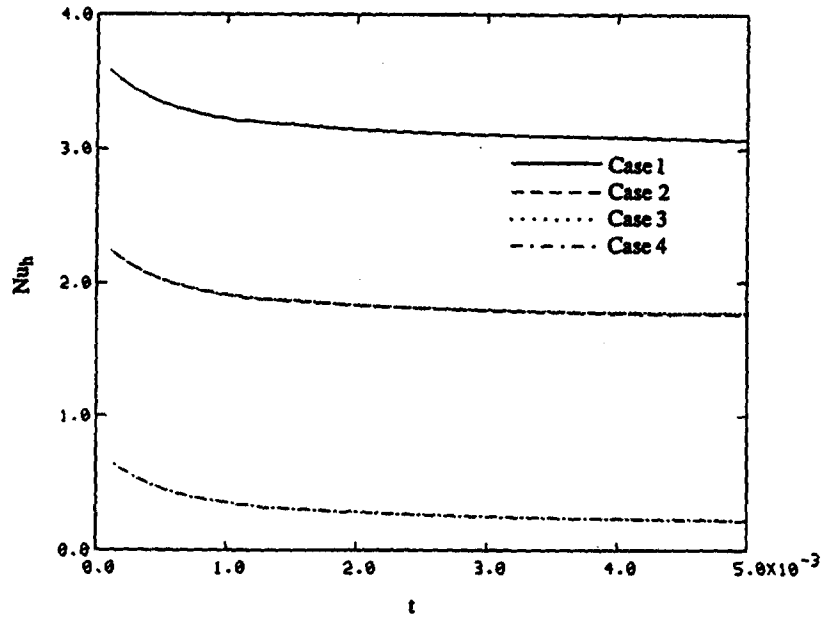

FIG. 15. The Nusselt numbers for the four cases corresponding to Fig. 1 for $B = 1000$, $B_v = 5 \times 10^4$ and an opening size of 1/4.

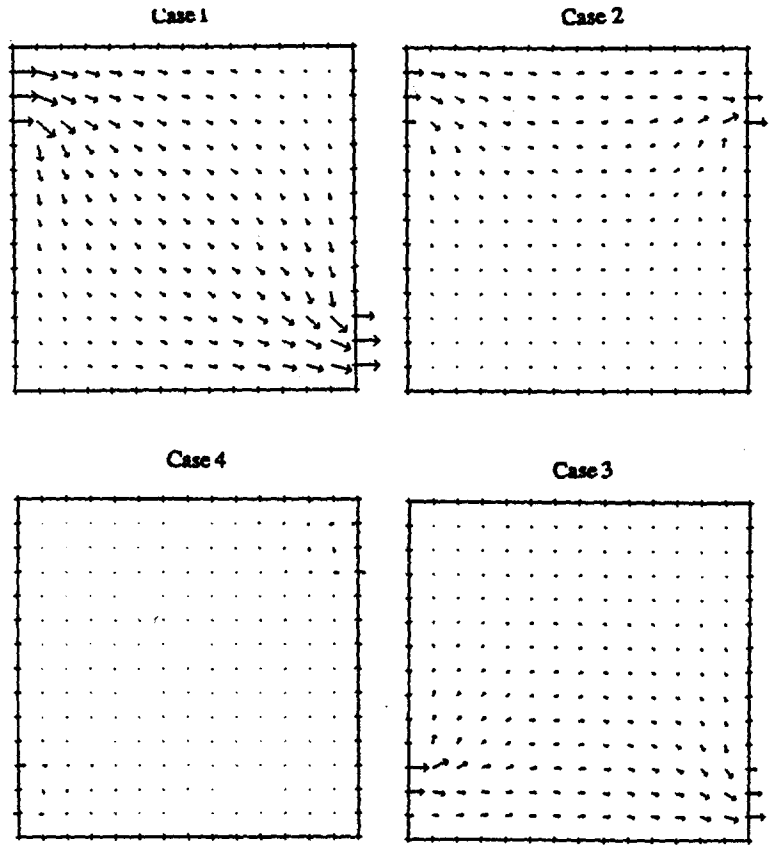

FIG. 16. Velocity distributions at t_3 for the four cases shown in Fig. 1 for $B = 1000$, $B_v = 5 \times 10^4$ and an opening size of 1/4.

Table 3. Effect of the pressure difference on the Nusselt number for case 1 with $B = 1000$, $B_v = 5 \times 10^4$, and an opening size ratio of 1/2

	Nu_h		
t	$\Delta p_\gamma = 10^{-5}$	$\Delta p_\gamma = 10^{-4}$	$\Delta p_\gamma = 10^{-3}$
0.0005	2.5444	14.826	135.94
0.001	2.4191	14.661	135.06
0.0015	2.3732	14.578	134.04
0.002	2.3360	14.532	132.90
0.0025	2.3130	14.491	132.37
0.003	2.2955	14.452	132.13
0.0035	2.2845	14.424	131.97
0.004	2.2740	14.397	131.80
0.0045	2.2646	14.374	131.72
0.005	2.2568	14.353	131.71

an increase in the Nusselt number. Also, an increase in the pressure difference will enhance the thermal penetration, vapor transport, condensation rate and the liquid content. For the sake of brevity, the field variable distributions for larger pressure differences are not presented here.

5. CONCLUSION

The air infiltration effects on heat transfer rates and the generated liquid condensate have been investigated in this work. The process was described by a system of intercoupled transport equations and several thermodynamic relations. An efficient finite difference scheme with a two-phase format was devised to solve the governing equations along with the convective boundary conditions. The important field variables, their subsequent interactions and the effects of the heat and mass transfer Biot numbers were investigated. Furthermore, the influence of the permeable region and the opening locations was systematically researched. In what follows some of the key conclusions are listed.

(1) The liquid accumulates much more in the region which is next to the hot and humid environment.

(2) Infiltration is the dominant mode of the overall heat transfer even in the presence of very small pressure gradients across the insulation slab.

(3) An increase in the heat transfer Biot number causes a subsequent increase in the Nusselt number.

(4) An increase in the mass transfer Biot number causes a subsequent increase in the Nusselt number at the initial stage. However, the reverse trend was observed at an intermediate stage.

(5) An increase in the opening area decreases the Nusselt number.

(6) The effects of the opening locations on the Nusselt number, velocity field, and the other field variables were found to be very significant.

Acknowledgement—The grant from Ohio Supercomputer Center is acknowledged and appreciated.

REFERENCES

1. J. R. Phillip and D. A. Devries, Moisture movement in porous materials under temperature gradients, *Trans. Am. Geophys. Union* **38**, 222–232 (1957).
2. D. A. Devries, Simultaneous transfer of heat and moisture in porous media, *Trans. Am. Geophys. Union* **39**, 909–916 (1958).
3. A. V. Luikov, System of differential equations of heat and mass transfer in capillary porous bodies (review), *Int. J. Heat Mass Transfer* **18**, 1–14 (1975).
4. S. Whitaker, Simultaneous heat, mass and momentum transfer in porous media: a theory of drying. In *Advances in Heat Transfer*, Vol. 13. Academic Press, New York (1977).
5. N. H. Ceaglske and O. Hougen, Drying granular solids, *Ind. Engng Chem.* **29**, 805–813 (1937).
6. D. Berger and D. C. T. Pei, Drying of hygroscopic capillary porous solids—a theoretical approach, *Int. J. Heat Mass Transfer* **16**, 293–302 (1973).
7. S. Whitaker and W. T.-H. Chou, Drying granular porous media—theory and experiment, *Drying Technol.* **1**, 3–33 (1983).
8. M. Kaviany and M. Mittal, Funicular state in drying of a porous slab, *Int. J. Heat Mass Transfer* **30**, 1407–1418 (1987).
9. G. B. Reddy, J. C. Mulligan and R. R. Johnson, Analysis of heat and mass transfer in unsaturated porous materials: an application to soil with a heat source, In *Multiphase Transport in Porous Media*, ASMEFED, Vol. 60, pp. 77–84 (1987).
10. K. S. Udell, Heat transfer in porous media considering phase change and capillarity—the heat pipe effect, *Int. J. Heat Mass Transfer* **28**, 485–495 (1985).
11. K. S. Udell and J. S. Fitch, Heat and mass transfer in capillary porous media considering evaporation/condensation and non-condensible gas effects. In *Heat Transfer in Porous and Particulate Flows*, ASMEHTD-Vol. 46, pp. 103–110 (1985).
12. E. R. G. Eckert and M. Faghri, A general analysis of moisture migration caused by temperature differences in an unsaturated porous medium, *Int. J. Heat Mass Transfer* **23**, 1613–1623 (1980).
13. H. A. Dinulescu and E. R. G. Eckert, Analysis of the one-dimensional moisture migration caused by temperature gradients in a porous medium, *Int. J. Heat Mass Transfer* **23**, 1069–1078 (1980).
14. R. P. Tye and S. C. Spinney, A study of the effects of the moisture vapor on the thermal transmittance characteristics of cellulose fibre thermal insulation, *J. Thermal Insulation* **2**, 175–196 (1979).
15. M. B. Stewart, An experimental approach to the study of moisture dynamics in walls, *ASTM STP* **779**, 92–101 (1982).
16. C. Langlais, M. Hyrien and S. Karlsfeld, Moisture migration in fibrous insulating material under the influence of a thermal gradient, *Moisture Migration in Building, ASTM STP* **779**, 191–206 (1982).
17. Y. Ogniewicz and C. L. Tien, Analysis of condensation in porous insulation, *Int. J. Heat Mass Transfer* **24**, 421–429 (1981).
18. K. Vafai and S. Sarkar, Condensation effects in a fibrous insulation slab, *J. Heat Transfer* **108**, 667–675 (1986).
19. K. Vafai and S. Whitaker, Heat and mass transfer accompanied by phase change in porous insulations, *J. Heat Transfer* **108**, 132–140 (1986).
20. P. J. Burns, L. C. Chow and C. L. Tien, Convection in a vertical slot filled with porous insulation, *Int. J. Heat Mass Transfer* **20**, 919–926 (1977).

21. P. J. Burns and C. L. Tien, Effects of infiltration on heat transfer through vertical slot porous insulation. In *Energy Conservation in Heat, Cooling, and Ventilating Buildings* (Edited by C. J. Hoogendoorn and N. H. Afgan), Vol. 1, pp. 93–105. Hemisphere, New York (1978).
22. C. Bankvall, Heat transfer in fibrous materials, *J. Testing Evaluation, JTEVA* **1**, 235–243 (1973).
23. C. Bankvall, Natural convection in vertical permeable space, *Wärme- und Stoffübertr.* **7**, 22–30 (1974).
24. P. Vasseur, T. H. Nguyen, L. Robillard and V. K. T. Thi, Natural convection between horizontal concentric cylinders filled with a porous layer with internal heat generation, *Int. J. Heat Mass Transfer* **27**, 337–349 (1984).
25. K. Vafai and C. L. Tien, Boundary and inertia effects on flow and heat transfer in porous media, *Int. J. Heat Mass Transfer* **24**, 195–203 (1981).
26. M. R. J. Wyllie, Relative permeability. In *Petroleum Production Handbook* (Edited by Frick), Vol. 2, Chap. 25. McGraw-Hill, New York (1962).
27. I. Fatt and W. A. Klikoff, Effect of fractional wettability on multiphase flow through porous media, AIME Technical Note No. 2043, *AIME Trans.* **216**, 426–432 (1959).

APPENDIX

The dimensionless variables are defined as

$$x = \frac{\bar{x}}{\bar{L}}, \quad y = \frac{\bar{y}}{\bar{L}}, \quad t = \frac{\bar{\alpha}_{\text{eff},0}\bar{t}}{\bar{L}^2} \tag{A1}$$

$$\mathbf{v}_\beta = \frac{\bar{\mathbf{v}}_\beta \bar{L}}{\bar{K}\bar{k}_\varepsilon/\bar{\mu}_\beta}; \quad \mathbf{v}_\gamma = \frac{\bar{\mathbf{v}}_\gamma}{\bar{v}_{\gamma,0}} \tag{A2}$$

$$T = \frac{\bar{T}}{\Delta\bar{T}}, \quad \dot{m} = \frac{\bar{m}\bar{L}^2\Delta\bar{h}_{\text{vap}}}{\bar{k}_{\text{eff},0}\Delta\bar{T}} \tag{A3}$$

$$\rho_j = \frac{\bar{\rho}_j}{\bar{\rho}_{j,0}}, \quad p_j = \frac{\bar{p}_j}{\bar{p}_{j,0}}, \quad \mathbf{g} = \frac{\bar{\mathbf{g}}}{\bar{\mathbf{g}}_0} \tag{A4}$$

and the dimensionless parameters are defined as

$$P_1 = \frac{\bar{\rho}_\beta}{\bar{\rho}_0}, \quad P_2 = \frac{\bar{c}_\beta}{\bar{c}_0}, \quad P_3 = \frac{\langle\bar{c}_\gamma\rangle^\gamma}{\bar{c}_0} \tag{A5}$$

$$P_4 = \frac{\bar{\rho}_{\gamma,0}}{\bar{\rho}_0}, \quad P_5 = \frac{\bar{\rho}_{\gamma,0}\bar{g}_0\bar{L}}{\bar{p}_{\gamma,0}}, \quad P_6 = \frac{\Delta\bar{h}_{\text{vap}}}{\bar{c}_0\Delta\bar{T}} \tag{A6}$$

$$P_9 = \frac{\Delta\bar{T}}{\bar{T}_0}, \quad P_{11} = \frac{\bar{\rho}_{v,0}}{\bar{\rho}_{\gamma,0}}, \quad P_{12} = \frac{\bar{\rho}_{a,0}}{\bar{\rho}_{\gamma,0}} \tag{A7}$$

$$P_{13} = \frac{\bar{\rho}_{v,0}}{\bar{\rho}_{\gamma,0}}, \quad P_{14} = \frac{\bar{\rho}_{a,0}}{\bar{\rho}_{\gamma,0}}, \quad P_{15} = \frac{2\bar{\sigma}_{\beta\gamma}}{\bar{r}\bar{\rho}_\beta\bar{R}_v\Delta\bar{T}} \tag{A8}$$

$$P_{16} = \frac{\Delta\bar{h}_{\text{vap}}}{\bar{R}_v\Delta\bar{T}}, \quad P_{18} = \frac{\bar{\alpha}_{\text{eff}}}{\bar{\alpha}_{\text{eff},0}}, \quad P_{19} = \frac{\bar{k}_{\text{eff}}}{\bar{k}_{\text{eff},0}} \tag{A9}$$

$$P_{20} = \frac{\bar{K}\bar{p}_{\gamma,0}}{\bar{\mu}_\gamma\bar{L}\bar{v}_{\gamma,0}}, \quad Pe = \frac{\bar{v}_{\gamma,0}\bar{L}}{\bar{\alpha}_{\text{eff},0}}, \quad Le = \frac{\bar{\alpha}_{\text{eff},0}}{\bar{D}_{v,\text{eff}}} \tag{A10}$$

$$\psi_T = \frac{\bar{k}_{\langle\gamma\rangle}\Delta\bar{T}}{\bar{k}_\varepsilon}, \quad \psi_g = \frac{(\bar{\rho}_\beta - \bar{\rho}_\gamma)\bar{g}_0\bar{L}}{\bar{k}_\varepsilon}, \quad \psi_\varepsilon = \frac{\bar{K}\bar{k}_\varepsilon}{\bar{\mu}_\beta\bar{\alpha}_{\text{eff},0}}. \tag{A11}$$

UNE SYNTHESE DE L'EFFET DE L'INFILTRATION SUR LA MATRICE D'ISOLATION

Résumé—On présente les effets de l'infiltration d'air sur le transfert de chaleur et de masse dans une matrice poreuse. Les frontières verticales du système poreux sont partiellement perméables de façon à simuler les trous ou les fissures dans les matériaux poreux d'isolation. Un schéma numérique efficace pour tenir compte du changement d'état est employé pour résoudre les équations appropriées avec les conditions aux limites qui décrivent les mécanismes compliqués de transport. On étudie les interactions des variables du champ et l'influence des nombres de Biot et de la taille d'ouverture. Les effets sur le nombre de Nusselt des positions des ouvertures sont étudiés pour quatre cas représentatifs. Dans tous les cas, on trouve que le liquide s'accumule bien dans la région exposée à l'environnement chaud et humide. On trouve aussi que l'infiltration joue un rôle très important dans la détermination des flux thermiques globaux aussi bien que dans celui du condensat liquide.

ZUSAMMENSETZUNG DER INFILTRATIONSEFFEKTE AN EINER WÄRMEDÄMMENDEN STRUKTUR

Zusammenfassung—Der Einfluß einer Infiltration von Luft auf den Wärme- und Stofftransport in einer porösen Matrix wird dargestellt. Die senkrechten Berandungen des porösen Systems werden als teilweise durchlässig angesehen, um Löcher oder Risse in dem porösen Wärmedämmaterial zu simulieren. Die maßgeblichen Gleichungen werden mit einem geeigneten numerischen Verfahren gelöst, das Phasenwechsel sowie die Randbedingungen für die komplizierten Transportvorgänge berücksichtigt. Die Wechselwirkung der Feldvariablen und der Einfluß der Biot-Zahl und der Öffnungsgröße werden untersucht. Die Einflüsse der Position der Öffnungen auf die Nusselt-Zahl werden anhand von vier repräsentativen Fällen untersucht. In allen Fällen ergibt sich, daß sich die Flüssigkeit vorwiegend in der Region ansammelt, die der heißen und feuchten Umgebung ausgesetzt ist. Außerdem zeigt sich, daß die Infiltration eine sehr wichtige Rolle bei der Bestimmung des Gesamtwärmedurchgangs wie auch der anfallenden Kondensatmenge spielt.

ОБОБЩЕНИЕ ФИЛЬТРАЦИОННЫХ ЭФФЕКТОВ В ИЗОЛЯЦИОННОЙ МАТРИЦЕ

Аннотация—Исследуется влияние фильтрации воздуха на тепло- и массоперенос в пористой матрице. Для моделирования отверстий или трещин в пористых изоляционных материалах вертикальные границы пористой системы считаются частично проницаемыми. Для решения соответствующих определяющих уравнений с граничными условиями, описывающими осложненный перенос, используется эффективная численная схема, учитывающая фазовый переход. Изучаются взаимодействие переменных поля, а также эффект чисел Био и размера отверстий. На примере четырех типичных случаев изучается влияние расположения отверстий на значение числа Нуссельта. Для всех случаев найдено, что большое количество жидкости накапливается в области, подверженной воздействию горячей и влажной окружающей среды. Найдено также, что фильтрация играет очень важную роль при определении скоростей суммарного теплопереноса, а также образующегося жидкого концентрата.